Superalloys 2012: 12th International Symposium on Superalloys
Edited by: Eric S. Huron, Roger C. Reed, Mark C. Hardy, Michael J. Mills, Rick E. Montero, Pedro D. Portella, Jack Telesman
TMS (The Minerals, Metals & Materials Society), 2012

FATIGUE CRACK PROPAGATION IN THIN-WALL SUPERALLOYS COMPONENT; EXPERIMENTAL INVESTIGATION VIA MINIATURE CT SPECIMEN

Motoki SAKAGUCHI [1], Takeshi TSURU [2], Masakazu OKAZAKI [2]
[1] Tokyo Institute of Technology, 2-12-1 Ookayama, Meguro-ku, Tokyo, Japan, 152-8552
[2] Nagaoka University of Technology, Kamitomioka-Machi 1603-1, Niigata, Japan, 940-2188

Keywords: Ni-base superalloy, Fatigue crack propagation, Miniature specimen, Grain boundary Crystallographic orientation, CMSX-4, IN939

Abstract

Fatigue crack propagation in thin-wall superalloys components were experimentally investigated at room temperature, employing miniature compact tension (CT) specimens directly extracted from an actual post-service gas turbine vane as well as as-cast single crystal and poly-crystal Ni-base superalloys. At first, the effect of crystallographic orientation on the fatigue crack propagation rate was investigated, using a single crystal Ni-base superalloy, CMSX-4, with different primary orientations. Based on the test results of the CMSX-4, some significant interactions between the crack and grain boundaries were discussed, using a conventional casting polycrystalline superalloy, IN939. Finally, the fatigue crack propagation resistance of the post-service gas turbine superalloy was examined, extracting the miniature CT specimens from the leading and trailing edge of the post-service vane. It was found from a series of investigations that the crack propagation rates in the miniature specimens were generally higher than those in the standard size specimen. It was also shown that the fatigue crack propagated with significantly higher rate in the trailing than in the leading edge. These findings were reasonably interpreted in terms of the crack propagation mode and grain boundary role, which were affected by the specimen thickness and the in-service damage in the actual gas turbine.

Introduction

High temperature components in advanced industrial gas turbines, such as blades or vanes, have to operate under a severe combination of mechanical and environmental loadings. This service condition inevitably causes many types of damage and degradation in components during the operation period. Materials used for them, especially Ni-base superalloys, are such expensive items that they can be a substantial part of an operating and a maintenance budget [1]. Therefore, it is of considerable technical and financial benefit if the condition of the blades can be assessed and their remaining life determined.

Whilst some efforts based on the crack assessment have been made to estimate the remaining life of superalloy component [2-9], there is not well-established information and methodologies. Some reasons are responsible for following problems:

i) Fatigue crack propagation (FCP) tests are usually carried out using standard size specimens (5-10mm thickness) [10], although actual crack growth takes place in thin wall components with cooling systems, where the wall thickness is about 0.5-1.0mm. The thickness dependency of crack propagation may lead to a discrepancy between the laboratory results and the actual crack growth [11].
ii) Little is known quantitatively about effects of both the crystal and grain boundary orientation [12,13]. These effects should become more significant in the thin-wall components because their dimensions are of same order as the grain size of the material.
iii) Time dependent degradation during the gas turbine operation, such as creep deformation, oxidation and microstructural evolution, interact with the above two problems and mutually make the phenomena more complicated [14].

The first objective in this study is to experimentally clarify fundamental features of FCP behavior in thin-wall components, employing a miniature compact tension (CT) specimen extracted from as-cast single crystal and conventional casting poly-crystal superalloy. The second objective is to assess the in-service damage in a post-service gas turbine vane through the FCP test for the miniature CT directly extracted from actual post-service vane. The present study flow consists of three stages. The first stage is to investigate the effect of crystallographic orientation on the FCP rate in single crystal superalloy specimens with different orientations. The second stage is to make clear the interaction between the crack propagation and grain boundaries in poly-crystalline superalloys. The third is to examine the FCP resistance of the post-service gas turbine superalloy through the FCP tests for miniature CT specimen extracted from the leading and trailing edge part in the post-service actual gas turbine vane, and to compare with the findings in the first and second stage approaches.

Experimental Procedures

Materials

Two kind of as-cast Ni-base superalloys were used in this study. One was a single crystal (SC) superalloy, CMSX-4, and the other was a conventional casting poly-crystalline (CC) superalloy, IN939. The chemical compositions and the heat treatment conditions of these superalloys are summarized in Table 1.

(a)

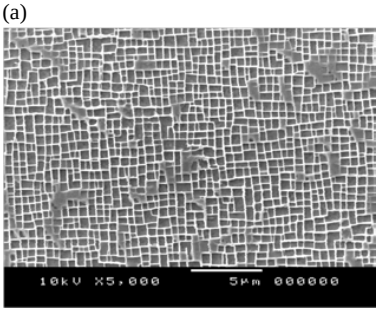

(b)

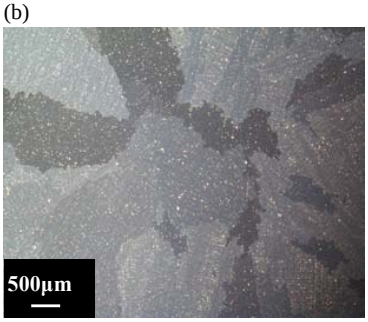

Fig.1 Microstructures of superalloys employed in this work.
(a) SEM image of single crystal superalloy, CMSX-4,
(b) optical image of poly-crystal superalloy, IN939

Table 1 Chemical compositions and heat treatments for superalloys employed in this study

CMSX-4

Al	Ti	Ta	Mo	W	Re	Hf	Cr	Co	Ni
5.7	1	6.5	0.6	6.4	2.9	0.1	6.4	9.7	Bal.

Solution treatment: 1277°C×2h + 1296°C×2h + 1304°C×3h+1313°C×3h+ 1316°C×3h + 1321°C×3h
Aging treatment: 1080°C×4h+880°C×20h

IN939

Cr	Co	C	W	Ti	Al	Nb	Ta	Zr	B	Ni
22.4	19	0.15	2	3.7	1.9	1	1.4	0.1	0.01	Bal.

Solution treatment: 1160°C×4h/RAC+1000°C×6h/RAC
Aging treatment: 900°C×24h/AC + 700°C×16h/AC

Microstructure in the CMSX-4 and IN939 are shown in Fig.1(a) and (b), respectively. In the CMSX-4, the size of cuboidal γ' precipitates and the volume fraction were approximately 0.5μm and 68%, respectively (Fig.1(a)). The average grain size of the IN939 was very large, ranging between from 1 to 3mm (Fig.1(b)).

A post-service gas turbine vane used in this study was fabricated by conventional casting and used for about 20000 hours as the 1st stage vane in a 1100°C -class land-base gas turbine made by Mitsui Engineering & Shipbuilding Co., LTD. The vane was made of a poly-crystalline superalloy, IN939. The overview and cross section of the vane are shown in Fig.2(a) and Fig.2(b),

(a)

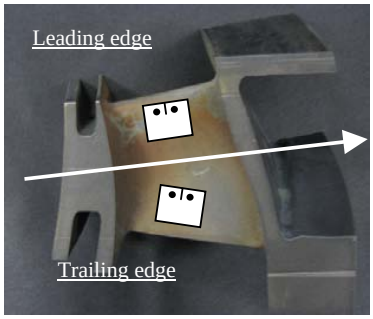

(b)

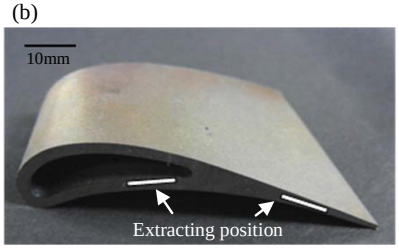

Fig.2 The post service gas turbine vane and how to extract the specimens. (a) Overview, (b) Transverse cross section of the vane and the site for the specimens extracted.

respectively. As shown in Fig.2(b) the vane has a thin wall structure associating with a simple inner air cooling system, where the wall thickness is from 1 to 3mm. As documented later in detail, miniature specimens were extracted from the vane for the FCP tests.

Preparation for miniature CT specimens

Miniature CT specimens were extracted from the cast rods of CMSX-4 and IN939. The geometry of the specimen, as shown in Fig.3, was designed so that it was almost proportional to that recommended in ASTM E647 [10], except for the specimen thickness. The experimental variables in the as-cast CMSX-4 specimen were primary crystal orientation of loading axis (that is, [100], [110] and [111] direction), as briefly summarized in Table 2. These orientations were not explicit but approximated with a mismatch within 5 degree. Hereinafter, the respective specimens are expressed to the name in Table 2. In the IN939, on the other hand, the miniature CT specimens were extracted from the center of cast rod so that the specimens belong to the RL orientation.

The miniature specimens were also extracted form the leading and the trailing edge part of the vane, as illustrated in Fig.2. All the specimens were prepared, according to the following procedures. At first, the plate pieces were extracted either from the core part of trailing edge or that of leading edge (on pressure side), and then the surface layer was removed by mechanical polishing so that the specimen did not include the aluminized area. Finally the CT specimen was machined from the plate piece by means of wire electro-discharge machining (EDM) with special care. Here an initial notch was introduced in such a direction that the fatigue crack propagated from the leading to trailing edge side in the crack propagation tests.

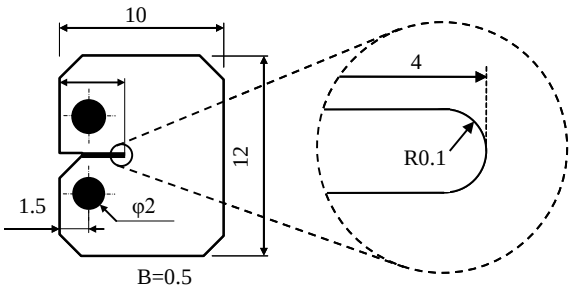

Fig.3 Geometry of a miniature CT specimen [mm]

Table 2 Tested specimens of as-cast CMSX-4

Specimen	Loading axis, L	T axis	P axis	Angle, θ (degree)	Angle, η (degree)	Fracture surface
100-1	[100]	[001]	[010]	45	45	(−11−1)
100-2	[100]	[001]	[010]	45	45	(−11−1)
110-1	[221]	[−110]	[114]	55	0	(−1−11)
110-2	[110]	[−11−2]	[−111]	22	58	(−1−11)
110-3	[110]	[00−1]	[−110]	0	35	(−1−11)
111-1	[111]	[−1−12]	[1−10]	68	55	(1−11)
111-2	[111]	[−1−12]	[1−10]	68	55	(−111)

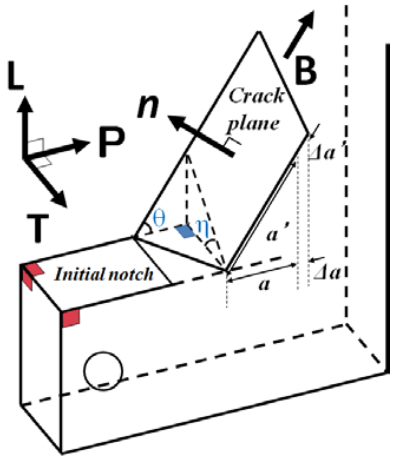

Fatigue crack propagation (FCP) tests

After all the specimens surface was polished to a mirror-like finish by emery papers and Al_2O_3 powder, fatigue crack propagation tests were carried out using a servo-electro hydraulic machine. Here, cyclic loading was applied to the miniature CT specimen through two loading pins at room temperature. The specimen was sandwiched between the two loading plates, which were useful to prevent out-of-plane deformation of the thin-wall specimen. During the tests, loading amplitude was kept constant under a loading frequency of 10 Hz with a loading ratio R=0.4 (defined by K_{min}/K_{max}, where K_{min} and K_{max} are minimum and maximum stress intensity factor during a cyclic loading, respectively). During the fatigue tests the crack length was monitored by means of a traveling microscope with a resolution of 5μm. The crack propagation rate, da/dN, was evaluated by the secant method. In order to minimize the effect of initial EDM notch, the crack growth behavior was analyzed after the crack length grew longer than 0.3 mm from the initial EDM notch root.

The stress intensity factor range, ΔK_{app}, was calculated, conforming to ASTM E647 [10];

$$\Delta K_{app} = F_I(\xi)\cdot\Delta\sigma^{\infty}\sqrt{\pi a} \qquad (1),$$

$$F_I(\xi) = \frac{1}{6\xi\sqrt{\pi}}(29.6 - 185.5\xi + 656\xi^2 - 1017\xi^3 + 639\xi^4)$$

$$\sigma^{\infty} = \frac{6\Delta P a}{BW^2}$$

$$\xi = a/W$$

Here, ΔP, B and W are load range, specimen thickness and width, respectively. However, as noted later, this treatment is no more than conventional, because the crack propagated along slip planes significantly deviating from macroscopic principal planes in this study, especially in the case of SC superalloy.

Results and Discussion

Fatigue crack propagation in the as-cast CMSX-4

FCP rates of the miniature CT specimens extracted from as-cast CMSX-4 are shown in Fig.4 as a function of the apparent stress intensity factor range (ΔK_{app}) . Here, FCP rates (da/dN) and ΔK_{app} were evaluated based on the incremental amount of projected crack length (Δa) normal to loading axis. It is found in Fig.4 that the rates are significantly depending on the specimen orientation, or loading axis direction. Generally speaking, a series of the [100] specimens revealed the highest rates, and the [111] specimens did the lowest, respectively. However, it should be noted that these dependencies are no more than an apparent tendency, because the treatment based on the ΔK_{app} and Δa does not take account of inclination angle of crack plane and intrinsic fracture mechanism.

The typical fracture surfaces of the specimens [100]-2 and [110]-2 are shown in Fig.5. Both fracture surfaces are significantly inclined to the loading axis, and revealed crystallographic features associating with the Stage I crack propagation. According to the fractographic analysis by SEM, the fracture surfaces in both specimens, as well as the other SC specimens, were composed of {111} crystallographic slip planes. However, the crack propagation path was depended on the specimens orientation; i.e., the cracks in the [100] and [111] specimens propagated along a single {111} slip plane (Fig.5(a)), while the crack in the [110] specimens frequently changed their planes from one type of {111} plane to another, and the resultant fracture surfaces were composed of multiple {111} slip planes with high asperities (Fig.5(b)). The geometrical features of the primary fracture plane are summarized in Table 2, where the features are represented by the inclined angles, θ and η; see an illustration in Table 2. Note that the fracture surfaces in the [110] specimens were composed of multiple slip planes as seen in Fig.5(b), hence the angles, θ and η, in Table 2 represent their measurement values of the most dominant fracture surfaces. Meanwhile, the fractographic analysis

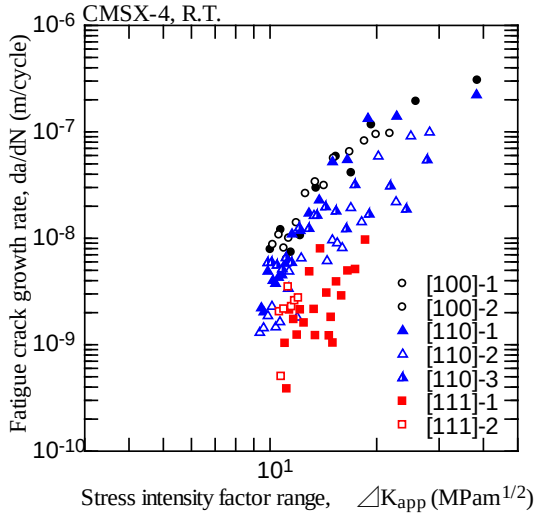

Fig.4 Crack propagation test result of single crystal superalloy, CMSX-4. Fatigue crack propagation rates (FCGRs) of [100], [110] and [111] specimens are plotted as a function of the Mode-I stress intensity factor range (ΔK_{app})

suggested that the FCP was driven by a shearing dominating mode along slip plane [5,9], and indicated that the apparent engineering treatment given in Fig.4 is not adequate.

Since the FCP in the SC superalloy was driven by a shearing dominating mode along the slip plane, the FCP behavior should be evaluated in terms of shear stress components on the actual {111} slip planes. In this study, a shear stress intensity factor range (ΔK_τ) was considered;

$$\Delta K_\tau = F_{III}(\xi)\cdot\Delta\tau\sqrt{\pi a'} \qquad (2),$$

$$F_{III}(\xi) = \sqrt{\frac{2}{\pi\xi}\tan(\frac{\pi\xi}{2})}$$

$$\Delta\tau = \Delta\sigma^{\infty}\cos\phi\cdot\sin\phi$$

Here, ϕ is an angle between slip plane normal, ***n***, and the loading axis. It should be noted that $\Delta\tau$ in eq.(2) is not a resolved shear stress taking account the slip direction, but a maximum shear stress on the slip plane. Such a treatment is useful in case the crack propagating direction cannot be strictly determined. In addition to the stress intensity factor, it is also preferable to convert the FCG rates (*da*/*dN*) that should be evaluated by the actual propagation rate based on incremental amount of fracture surface area by crack advance. While this type strict conversion is impossible so far as the crack plane is explicitly expressed, it is possible to estimate the most plausible value; that must be given by,

$$\Delta A \approx \frac{\Delta a}{\cos\theta\cdot\cos\eta} \qquad (3),$$

(a) [100]2

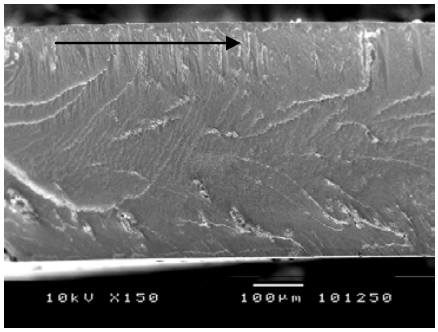

(b) [110]2

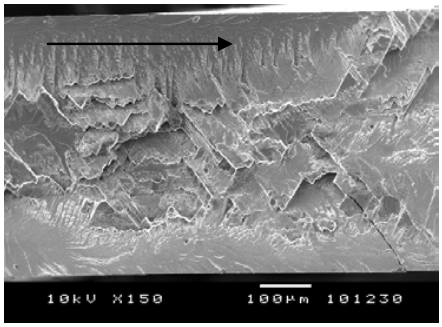

Fig.5 Fracture surface of miniature CT specimens of single crystal superalloy, CMSX-4.
(a) [100]-2 specimen and (b) [110]-2 specimen

where θ and η are angles representing fracture plane surface (see an illustration in Table 2), and Δa is an incremental amount of projected crack length to calculate *da*/*dN* in the experiment.

The relationship between *dA*/*dN* and ΔK_τ are given in Fig.6. Here, converted FCP rates in the miniature samples are compared with the FCP rates in the standard size CT specimen oriented to [100] direction, which were obtained by Telesman [5] based on the resolved shear stress intensity factor range (ΔK_{rss}). Comparing Fig.6 with Fig.4, it is found that the dependence of primary crystallographic orientation in the miniature specimens seems to be less when *dA*/*dN* is correlated with ΔK_τ. This means that the FCP behavior as well as their rates were controlled by shear mode in this work, and agrees with the findings by Telesman [5]. Focusing on the specimen thickness effect on the FCP rates in Fig.6, on the other hands, the FCP in the miniature specimens, especially in the [100] and [111] specimens, are significantly higher than that in the standard specimen. Such a specimen thickness dependency was mainly attributed to the difference in crack propagation mode; i.e., the cracks in the miniature [100] and [111] specimen propagated along a single slip plane, while cracks in the standard specimen propagated along multiple slip planes with frequently changing their advancing planes [5]. The crack plane transition and the crack path tilting associated with the latter types crack propagation usually reduces the effective driving force for crack growth and results in the crack retardation [12,13]. Similarly, the miniature [110] specimen, in which the fracture

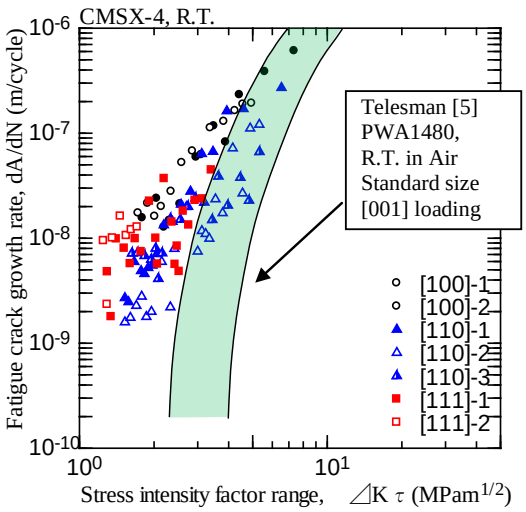

Fig.6 Crack propagation test result of single crystal superalloy, CMSX-4. Fatigue crack propagation rates of [100], [110] and [111] specimens are plotted as a function of the resolved shear stress intensity factor range (ΔK_τ)

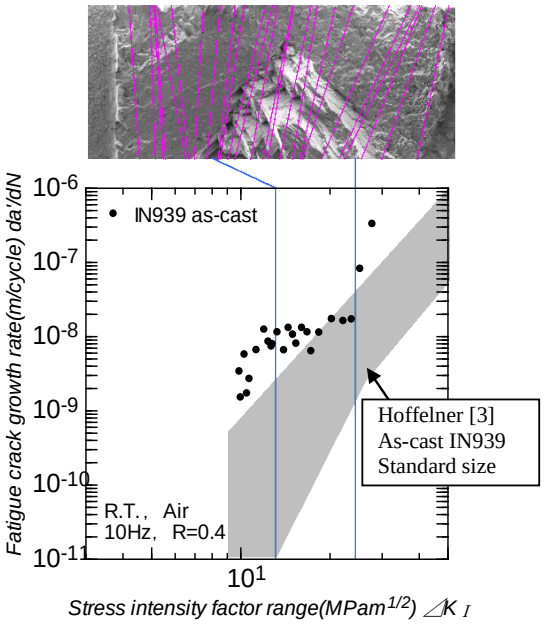

Fig.7 Test results of poly crystalline superalloy, IN939. Fatigue crack propagation rates are plotted as a function of the Mode I stress intensity factor range (ΔK_{app}).

surface was composed of multiple slip planes as in Fig.5(b), reveals lower FCP rates than those of [100] and [111] specimens.

Fatigue crack propagation in the as-cast IN939

The FCPR of the as-cast poly-crystalline superalloy, IN939, is revealed in Fig.7 as a function of the apparent stress intensity factor range (ΔK_{app}), together with a data band for standard size specimens [3]. The corresponding crack surface of the miniature specimen is also shown in Fig.7, in which some straight lines are drawn to reveal how the tentative crack front on the specimen surfaces changed with the crack propagation. This kind of analysis enabled us to understand easily how the crack propagated. First of all, it is found in Fig.7 that the FCP rate of the miniature specimen is higher than that of the standard specimen. One of the contributing factors for this size dependency was a difference in crack propagation mode between the miniature and standard specimen. As easily supposed from the fracture surface in the miniature specimen, the fatigue fracture was driven only by two grains in Fig.7. Such a situation is not special but quite normal in this study, because the grain size of as-cast IN939 is often of the same order as the thickness of the miniature specimen. According to the crystallographic analysis, the two grains appearing in Fig.7 had the following primary orientations to loading axis approximately: the grain near an initial notch had <100> orientation, and at the middle it had a near <110> orientation, respectively. It is seen in Fig.7 that the FCP rates propagating for the <100> orientation grain gradually saturated as the crack front approached to the <110> grain; i.e., as it passed through the grain boundary. It is also found that the FCP rates were still lower after the crack front partially penetrated into the neighboring <110> grain: see Regime B. It is worthwhile to consider again that the [110] specimens had higher crack propagation resistance than the [100] specimen as in Fig. 6. Thus, such a change in FCP rates from the Regime A and B is expected. It is also noted in Fig.7 that when the crack penetrated into the <110> grain, the crack front noticeably deflected, or changed its propagation direction. This kind of deflection seems to be responsible for the transient behavior near the grain boundary. In the other words, the grain boundary between the <100> and <110> grains in this specimen acted as obstacles to retard the crack propagation [12,13]. Therefore, it is quite natural to consider that the size dependency of FCP rate is relevant to a difference in the number of grain boundaries and also relevant to a resultant difference in the crack propagation mode.

Although many other contributing factors might be responsible for the size effects on the FCP rates in the CMSX-4 and the IN939, it is practically important to keep in mind that the size effect seen in Fig.5 and Fig.6 leads to non-conservative life estimation for thin-wall superalloy components.

Fatigue crack propagation in the post-service vane

Before the results of FCP tests, metallography of the post-service gas turbine vane should be represented. Figure 8 summarizes the microstructures in the leading edge and the trailing edge from a macroscopic or microscopic level. Roughly speaking the grain size was of the order of millimeters, as is often the case in conventionally cast Ni-base superalloys. It is found in Fig.7 that the grain size in the trailing edge (Fig.8(a)) is significantly smaller than that in the leading edge (Fig.8(b)). This grain size

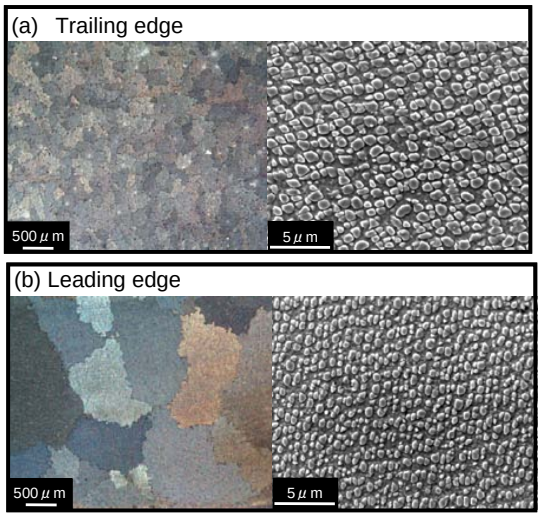

Fig.8 Metallurgical view of the vane from macroscopic (left photo) and microscopic (right photo) level.

distribution might result from a difference in cooling rate during the cast process of the original vane and not the result of the in-service period of gas turbines. Focusing on the higher magnification pictures in Fig. 8, it is seen that the volume fraction of γ' precipitates; the strengthening precipitates in Ni-base superalloys, were almost comparable between the respective areas. However, the size of γ' was relatively larger and more spheroidized in the trailing edge, compared with that in the leading edge part. This suggests that the aging damage would be more significant at the trailing edge part than that at the leading edge.

The FCP rates of the post-service vane at room temperature are correlated with the apparent stress intensity factor range (ΔK_{app}), in Fig.9. For a comparison, the FCP rates in the miniature as-cast IN939, as already shown in Fig.7, are also plotted in Fig.9. It is found in Fig.9 that the crack propagating at the trailing edge reveals higher rate by several orders of magnitude compared with that propagating at the leading edge part, especially under high ΔK regime. In addition, the rates in the trailing edge are higher than those of the as-cast IN939 specimen, while the rates in the leading edge part are almost comparable. Unfortunately, the virgin IN 939 vane was not available in this study; hence, it is difficult to explicitly confirm the reason for the higher FCP rate at the trailing edge. However, it is reasonable to consider the difference between the leading and the trailing edge would be mainly attributed to an in-service damage during the long term operation at elevated temperature, which might induce grain boundary oxidation or embrittlement and resulted in a reduction of the capability to prevent the crack propagation [14]. Indeed, the FCP rate in the trailing edge specimen was not reduced even when the crack front passed through grain boundaries, while the crack retardation was observed in the leading edge specimen similar to that in the as-cast IN939 specimen shown in Fig.7. Therefore, a treatment to recover the crack retardation role of grain boundary should

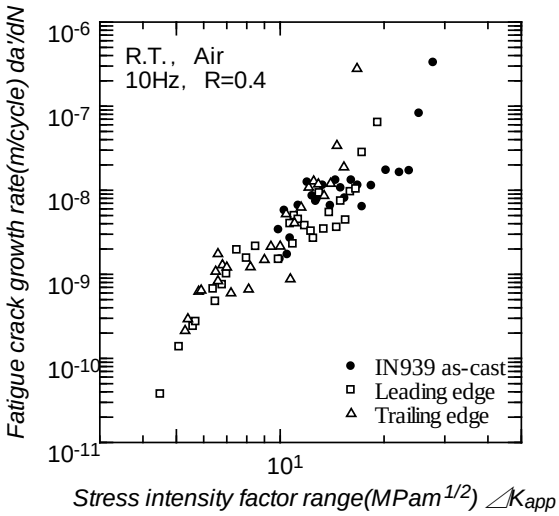

Fig.9 Fatigue crack propagation rates of the post-service vane. The FCP rate in the trailing edge is higher than the leading edge and the as-cast IN939.

improve the crack propagation resistance in the post-service gas turbine vane.

Summary

Fatigue crack propagations in thin-wall superalloys components were experimentally investigated, employing miniature compact tension (CT) specimens directly extracted from an actual post-service gas turbine vane as well as as-cast single crystal and poly-crystalline Ni-base superalloys. Special focus was put on the effect of crystallographic orientation, grain boundaries and in-service damage of gas turbine. The conclusions derived from a series of experiments are summarized as follows:

(1) In the single crystal superalloy, CMSX-4, the fatigue crack propagation rates in the [110] specimens were lower than those in [100] and [111] specimens, when the propagation rates were correlated with a parameter to represent stress intensity for shear mode fracture.

(2) In both the as-cast single crystal superalloy, CMSX-4, and the poly-crystalline superalloy, IN939, the fatigue crack propagation rates (FCPRs) in the miniature specimens were significantly higher than those in the standard size specimen. A predominant contributing factor for the size dependency was reasonably interpreted in terms of the crack propagation mode and the role of grain boundaries.

(3) In the post-service gas turbine vane, the fatigue crack propagation rate in the trailing edge specimen was higher than the as-cast and leading edge specimens. This is mainly attributed to an in-service damage during the long term operation at elevated temperature.

Acknowledgements

Financial support by Research Seeds Quest Program from JST and Grant-in Aid for Scientific Research from JSPS (No. 21246022) is greatly acknowledged.

References

[1] Schafrik. R. E., and Walston. S., Superalloys 2008, edited by R.C. Reed, K.A. Green, P. Caron, T.P. Gabb, M.G. Fahrmann, E.C. Huron, S.A. Woodard, "Challenges for high temperature material in the new millennium", TMS, (2008), pp. 3-9

[2] R.B.Scarlin, "Fatigue crack growth in a cast Ni-base alloy", Materials Science and Engineering, Vol.21, pp.139-147, (1975)

[3] W. Hoffelner, "High-cycle fatigue-life of the cast nickel base-superalloys IN 738 LC and IN 939", Metallurgical Transactions A, Vol.13A, pp.1245-1255, (1982)

[4] R.B.Scarlin, "Fatigue crack propagation in a directionally-solidified nickel-base alloy", Metallurgical Transactions A, Vol.7A, pp.1535-1541, (1979)

[5] J.Telesman, L.J.Ghosn, "The unusual near-threshold FCG behavior of a single crystal superalloy and the resolved shear stress as the crack driving force", Engineering Fracture Mechanics, Vol.34, No.5/6, pp.1183-1196, (1989)

[6] B.F.Antolovich, A.Saxena, S.D.Antolovich, "Fatigue Crack Propagation in Single-Crystal CMSX-2 at Elevated Temperature", Journal of Materials Engineering and Performance, Vol.2(4), pp.489-495, (1993)

[7] M. Okazaki, T.Tabata, S.Nohmi, "Intrinsic Stage I crack growth of directionally-solidified Ni-base superalloys during low-cycle fatigue at elevated temperature", Metall. Trans., Vol.21A, (1990), pp.2201-2209

[8] H.B.Henderson, J.W.Martin, "The influence of crystal orientation on the high temperature fatigue crack growth of a Ni-based single crystal superalloy", Acta mater. Vol.44, No.1, (1996), pp.111-126

[9] D.A.Koss, K.S.Chan, "Fracture along planar slip bands", Acta metal., Vol.28, (1980), pp. 1245-1252

[10] Annual Book of ASTM Standards, E647-00, Vol.03.01, ASTM International, (2003), pp.615-641

[11] M.Sakaguchi, M.Okazaki, Y.Sasaki, K.Namba, "Evaluation of Fatigue Crack Propagation in The Post-Service Gas Turbine Vane", Jounal of Solid Mechanics and Materials Engineering, Vol.4, No.2, (2010), pp.131-142

[12] T.Zhai, A.J.Wilkinson, J.W.Martin, "A crystallographic mechanism for fatigue crack propagation through grain boundaries", Acta mater., Vol.48, (2000), pp.4917-4927

[13] W.Schaef, M.Marx, H.Vehoff, A.Heckl, P.Randelzhofer, "A 3-D view on the mechanisms of short fatigue cracks interacting with grain boundaries", Acta Materialia, Vol. 59, (2011), pp.1849-1861

[14] W.M.Kane, U.Krupp, C.J.McMahon Jr, "Anisotropy of cracking from oxygen-induced dynamic embrittlement in bicrystals of IN718", Materials Science and Engineering A, Vol.507, Nno.1-2, (2009), pp.58-60